

OBSERVABLE QPOS PRODUCED BY STEEP PULSE PROFILES IN MAGNETAR FLARES

C. R. D'ANGELO AND A. L. WATTS

Instituut Anton Pannekoek, University of Amsterdam, Amsterdam 1098 XH, The Netherlands

Draft version September 12, 2021

ABSTRACT

Strong quasi-periodic oscillations (QPOs) in the tails of the giant gamma-ray flares seen in SGR 1806–20 and SGR 1900+14 are thought to be produced by starquakes in the flaring magnetar. However, the large fractional amplitudes (up to $\sim 20\%$) observed are difficult to reconcile with predicted amplitudes of starquakes. Here we demonstrate that the steeply pulsed emission profile in the tail of the giant flare can enhance the observed amplitude of the underlying oscillation, analogously to a beam of light oscillating in and out of the line of sight. This mechanism will also broaden the feature in the power spectrum and introduce power at harmonics of the oscillation. The observed strength of the oscillation depends on the amplitude of the underlying starquake, the orientation and location of the emission on the surface of the star, and the gradient of the light curve profile. While the amplification of the signal can be significant, we demonstrate that, even with uncertainties in the emission geometry, this effect is not sufficient to produce the observed QPOs. This result excludes the direct observation of a starquake and suggests that the observed variations come from modulations in the intensity of the emission.

Subject headings: pulsars: individual (SGR 1806–20, SGR 1900+14), stars: magnetars, stars: oscillations, X-rays: stars

1. INTRODUCTION

Giant gamma-ray flares are thought to be produced by a large-scale rearrangement of the super-strong magnetic field of a magnetar (Thompson & Duncan 1995, 2001). The large amount of energy released during a flare ($\sim 10^{46}$ erg) likely triggers large-scale vibrations and quakes in the star's crust (Duncan 1998). The observation of strong, long-lived quasi-periodic oscillations (QPOs) in the decay tails of the giant flares of SGR 1900+14 and SGR 1806–20 has been interpreted as evidence of such starquakes (Israel et al. 2005; Strohmayer & Watts 2005; Watts & Strohmayer 2006; Strohmayer & Watts 2006; hereafter SW06), and much theoretical work has subsequently focused on the physics of starquakes themselves (e.g., Levin 2006; Glampedakis et al. 2006; Gabler et al. 2011, for a recent review see Watts 2011).

Comparatively little work has focused on how the physical motion of the crust translates into a detectable QPO (although see Timokhin et al. 2008). This is not a trivial question: some of the QPOs have rms fractional amplitudes of up to 20% of the total flux in a pulse, whereas the maximum predicted amplitude of a starquake (assuming the oscillation is restricted to the crust) is about $0.01R_*$ (where R_* is the stellar radius). A persistent starquake will more likely have an amplitude at least $10\times$ smaller (Duncan 1998; Levin & van Hoven 2011; M. Gabler, 2012 private communication).

A solution could come from the steeply peaked pulse profile in the magnetar tail (see the pulse profile for SGR 1806–20 in Figure 4). The observed QPOs are phase dependent, and are sometimes centered on the steep edge of the pulse (e.g., Figure 3 of Strohmayer & Watts 2005). Strohmayer & Watts (2005) suggested that beamed emission could enhance the observed strength of an underlying oscillation. As the beam edge sweeps through the observer's line of sight, the underlying starquake will cause the edge to wiggle in and out of the observer's line of sight and amplify the signal.

In this Letter we use a toy model for the emission to quan-

tify the effect that the pulse shape will have on an underlying small-amplitude oscillation. The observed oscillation depends strongly both on the pulse profile and its orientation on the surface of the star. We demonstrate that the observed oscillation can easily be several times larger than the underlying physical motion from a starquake. However, the enhancement is likely not enough to fully explain the observed amplitudes of the QPOs in SGR 1806–20 and SGR 1900+14, suggesting that the observed oscillations are produced by a changing intensity in the emission rather than physical motion of the beam itself.

2. MODEL FOR STARQUAKE

To quantify how the signal from a starquake will be modified by the pulse profile requires a description for the oscillation and the emission. We adopt a simplistic model for both the emission and oscillation geometry, and further assume that the emission comes from close to the star's surface and moves with the crust. This can easily be generalized to a more detailed two-dimensional model for both the crust motion and the pulse pattern.

Figure 1 shows a sketch of the star. The star rotates with frequency Ω_* about the z -axis, which is inclined by angle i from the observer's line of sight. The dashed line shows the observer's viewing parallel: rays parallel to the surface normal on the viewing parallel will be observable. Assuming the emission is strongly beamed (necessary to produce sharp gradients), the emission from the star will be visible where it crosses the viewing parallel. We assume that the emission beam is a narrow strip in which the intensity varies strongly across the strip but stays roughly constant along it. The beam is seen in close-up in the figure and the line density shows the changing emission intensity.

An oscillation with frequency ν_0 (where $\nu_0 \gg \Omega_*$) and physical displacement Δx is superposed on top of the star's overall rotation. The orientation can be random however we consider only the component perpendicular to the beam's gradient, since an oscillation along the gradient will not change

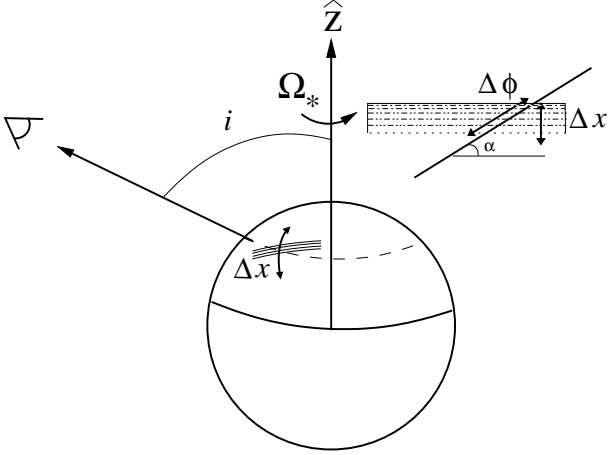


FIG. 1.— Sketch of star with starquake. Main: the star rotates at Ω_* , with a starquake with amplitude Δx superposed on the rotation. The dashed line shows the observer’s viewing parallel (at inclination i). The beam is observed (parallel lines on the star’s surface) where it crosses the viewing parallel. Inset: the viewing parallel (solid line) crosses the beam at angle α . A physical motion Δx is observed as a change in phase $\Delta\phi$, which can be large if α is small.

the emission profile. The beam crosses the viewing parallel with angle α , so the observed pulse profile is somewhat broadened.

The high-frequency oscillation Δx corresponds to a shift in the rotation phase, $\Delta\Phi$:

$$\Delta\Phi = \frac{\Delta x}{R_* \sin i \sin \alpha} \sin(2\pi\nu_0 t). \quad (1)$$

The $1/\sin \alpha$ term arises from the misalignment between the beam and viewing parallel. As the beam oscillates in direction Δx , the change in flux corresponds to a shift in rotation phase $\Delta\phi$ larger than the physical displacement. This is because the observed beam is broadened along the viewing parallel, while Δx probes the ‘true’ beam profile¹. Angles α and i are unknown: however, we will argue later that they are insufficient to amplify a starquake into the observed features.

Using the emission profile, $P(\Phi_0)$, we can calculate $P(\Phi)$ and see how the starquake changes the overall variability in the light curve. Since $\Delta\Phi$ is small, observed profile is:

$$\begin{aligned} P(\Phi) &= P(\Phi_0 + \Delta\Phi) \\ &= P(\Phi_0) + \Delta\Phi \left. \frac{dP}{d\Phi} \right|_{\Phi_0} + \mathcal{O}(\Delta\Phi^2). \end{aligned} \quad (2)$$

When the gradient of the light curve is large ($\sim P(\Phi_0)/\langle\Delta\Phi\rangle$), the starquake will be boosted and dominate the light curve.

This process will have two other effects on the observed variability. First, since $\frac{dP}{d\Phi}$ changes, the observed amplitude of the oscillation varies, which will redistribute the signal power at ν_0 into a range of frequencies. The width of the signal in the power spectrum can be estimated from the rate of change in the observed oscillation amplitude, i.e., $\frac{d^2P}{d\Phi^2}$. This process will also introduce harmonics of ν_0 into the light curve.

In summary: the strength of the oscillation seen by the viewer depends on Δx , i , α and $\left. \frac{dP}{d\Phi} \right|_{\Phi_0}$. $\left. \frac{d^2P}{d\Phi^2} \right|_{\Phi_0}$ determines the width and shape of the feature in the power spectrum, as well as the magnitude of harmonics of ν_0 .

¹ We are grateful to Yuri Levin for pointing this additional geometrical factor out to us.

2.1. Making a Periodic Signal Quasi-Periodic

The high-frequency signals detected in SGR 1806–20 and SGR 1900+14 had resolved widths suggesting that the underlying oscillation is not a purely periodic signal. To understand how the pulse profile changes a signal with a range of frequencies, we add QPOs to the light curve of SGR 1806–20.

We model QPOs as noise processes with a Lorentzian distribution of powers as input following the method suggested by Timmer & Koenig (1995). The power spectrum of the QPO in rms normalization (e.g., van der Klis 1989) is given by:

$$S_{\text{QPO}} = \frac{\sigma^2 \Delta f_{\text{Ny}}}{2\pi} \frac{1}{(\Delta/2)^2 + (\nu - \nu_0)^2}. \quad (3)$$

In Equation (3), f_{Ny} is the Nyquist frequency, σ^2 is the QPO variance, Δ is its full-width at half-maximum (FWHM), and ν_0 is its central frequency.

The total power of the QPO is the same as for a sinusoid, only distributed over a range of frequencies. The variance of $F(t) = A_0 \sin(2\pi\nu_0 t)$ over time interval T is:

$$\sigma^2 = \frac{A_0^2}{T} \int_0^T dt \sin^2(2\pi\nu_0 t) = \frac{A_0^2}{2}, \quad (4)$$

so that substituting the amplitude from Equation (1), σ^2 in Equation (3) is given by:

$$\sigma^2 = \frac{1}{2} \left(\frac{\Delta x}{R_* \sin i \sin \alpha} \right)^2. \quad (5)$$

To produce a time series of length T , we generate a realization of its Fourier transform by taking the power (Equation (3)) at each frequency, $\nu_n \equiv n\Delta\nu$ ($\Delta\nu \equiv 1/T$) and multiplying by a complex number ($A_n + iB_n$) whose real and imaginary parts are drawn from a Gaussian random distribution with a variance of one and mean of zero:

$$f_n = (A_n + iB_n) \sqrt{\frac{1}{2} S_{\text{QPO}}(\nu_n)}. \quad (6)$$

The resulting time series has a variance σ^2 and a mean of zero. This signal is the offset $\Delta\Phi$ to the star’s phase Φ_0 as a function of time.

2.2. Example: A Power Law Light Curve

We illustrate how the pulse profile changes an underlying oscillation with an emission profile $P(\Phi_0) \propto \Phi_0^\beta$, adopting different values of β . This idealized shape corresponds roughly to the edges of the pulse where QPOs have been observed.

We use the same total flux for each profile, and neglect the effect of shot noise. We adopt a period of 10 s for the emission duration a time resolution of $\Delta t = 9.5 \times 10^{-6}$ s. We add a sinusoidal oscillation to the rotation phase, with amplitude $\Delta x/R_* \sin i \sin \alpha = 0.1$ and frequency $\nu_0 = 600$ Hz.

Figure 2 shows the power spectra around 600 Hz, for $\beta = [1, 2, 4, 8]$, increasing from bottom to top. The inset of Figure 2 shows the different emission profiles. The rms variability from the starquake is measured by integrating the spectrum in an interval of 30 Hz centered at 600 Hz and subtracting the power contribution from the underlying emission profile.

The main effect of steeper profiles is to increase the rms variability of the starquake. For $\beta = 1$, the oscillation is a

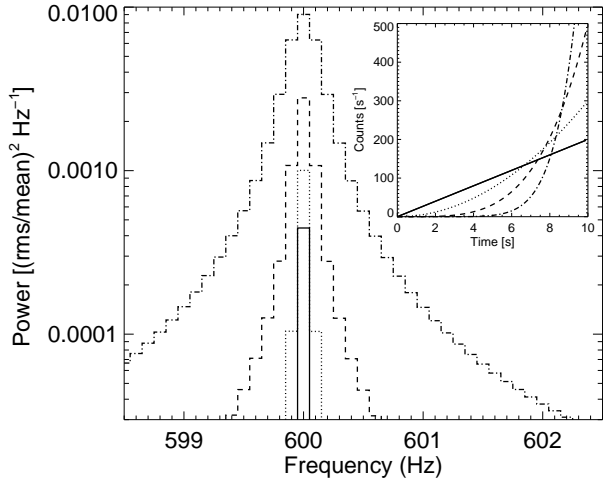


FIG. 2.— Main: power spectra centered around high-frequency feature for (bottom to top) $\beta = [1, 2, 4, 8]$. The gradient in the light curve determines the width and amplitude of the resulting feature. Inset: the emission profile for each power spectrum. Solid: $\beta = 1$; dotted: $\beta = 2$; dashed: $\beta = 4$; dot-dashed: $\beta = 8$.

TABLE 1
PROPERTIES OF OSCILLATION IN POWER-LAW LIGHT CURVE

β	ν_0 (Hz)	Width (Hz)	rms Fundamental	rms 1st harmonic
1	600	...	2.2%	0
2	600	0.11	2.9%	$2.7 \times 10^{-4}\%$
4	600	0.162	8.4%	$1.2 \times 10^{-3}\%$
8	600	0.3	20.5%	$6.1 \times 10^{-3}\%$

spike at 600 Hz with an rms amplitude of $\sim 2\%$. As β increases, the amplitude and width of the feature increase, so that for $\beta = 8$ the feature has an rms amplitude of $\sim 20\%$ —a ten-fold increase.

For larger β , the gradient of $P(\Phi_0)$ also changes substantially, which broadens the feature so that the FWHM for $\beta = 8$ is 0.3 Hz. The full properties of the signal for each β are summarized in Table 1.

From the generated power spectrum we also measure the starquake harmonics. The last column of Table 1 shows the rms of the first harmonic (at 1200 Hz) for different β . Even for $\beta = 8$, the power in the first harmonic is much smaller than the fundamental and would not be detectable above photon noise.

These results show that a small oscillation can be substantially increased by a steep gradient of the light curve. We next apply the same technique to the light curve of SGR 1806–20, to demonstrate how the beam shape will affect the oscillation amplitude.

3. THE TAIL OF SGR 1806–20

The tail of the 2004 giant flare of SGR 1806–20 showed strongly pulsed emission with two main peaks in the pulse profile. QPOs appeared at different phases in the pulse profile, and also lasted for different lengths of time (Watts & Strohmayer 2006, SW06). Two of the strongest QPOs, one at ~ 90 Hz and one at ~ 625 Hz are associated with steep gradients in the pulse profile. A dynamic power spectrum of the data showed that the 625 Hz QPO is strongest

in the declining edge of the pulse (Figure 3 of SW06). We therefore focus our study on the same phase as in SW06.

SW06 found phase-dependent QPOs at 93 Hz and 625 Hz in the SGR 1806–20 giant flare beginning 195 s after the main spike. The inset of Figure 4 shows the averaged pulse profile for the nine subsequent rotation cycles, and the solid lines show the phase segment when the QPOs were detected most strongly.

A starquake will only be boosted by rotation-dependent variation of the light curve. The *RXTE* data of SGR 1806–20 shows substantial variability, particularly below 100 Hz, but the rotation period of the star is closer to 0.1 Hz. Additionally, at shorter time bins the signal-to-noise ratio drops and the variability from photon noise dominates. We thus bin and smooth the entire light curve to a time resolution of 0.1 s, removing signal power at frequencies above ~ 10 Hz.

Since the resulting feature depends on the gradient of the pulse profile and its derivative (Equation (2)), the binsize and smoothing change the detailed shape and intensity of the feature. Experimenting with different binsizes and smoothing prescriptions shows the amplitude of the feature is robust (to $\sim 10 - 20\%$) to changes. The width and shape of the feature are more sensitive to higher derivatives so that the widths and the shapes of the features we produce serve more as qualitative examples than quantitative results.

To probe the effect of the pulse shape on the output oscillation strength, we make a light curve with two features, with $\Delta\Phi = 0.1 \sin(2\pi\nu_0 t)$ at $\nu_0 = 90$ Hz and at $\nu_0 = 625$ Hz. We then follow SW06 and examine the light curve 195–260 s after the main flare, calculating the power spectrum of the 3 s phase segment shown in the inset of Figure 4. The rms amplitude of the signal changes between rotations (from the changing pulse profile) from 16% to 25%. Stacking and averaging the power spectra we measure the average power in each feature. The stacked power spectrum centered around 90 Hz is shown in Figure 3. The feature has an amplitude of 21% and FWHM width of 1.6 Hz. The feature at 625 Hz has an rms amplitude of 20% and width 1.6 Hz. While the width is still smaller than the widths of the measured features (1.8 Hz for the 625 Hz feature and 8.8 Hz for the 93 Hz feature; SW06), it nonetheless demonstrates that a very narrow feature can be substantially broadened by the light curve profile.

The harmonics of the features are stronger than for the power-law case with an rms amplitude of 3% and a large frequency spread in the first harmonic. This is still undetectable, even when the oscillation has an observed rms amplitude of 20%.

3.1. QPOs in SGR 1806–20

The QPO features detected in SGR 1806–20 have measurable widths between 1–17 Hz, and frequencies where photon noise dominates the variability. Both these effects can change the measured properties of QPO, as we study below. We model the starquake as a quasi-periodic signal as outlined in Section 2.1, defining an input width, central frequency and amplitude. To simulate photon noise we use the output light curve as a probability function to detect a photon in a given time bin and generate a light curve as a series of discrete events. Since these are both random noise processes, we generate a large number of realizations and measure the QPO properties statistically.

As above, we add two QPOs to the phase of the SGR 1806–20 light curve and calculate the modified profile. One QPO is centered at 93 Hz with a width of 6 Hz, the second at 625 Hz

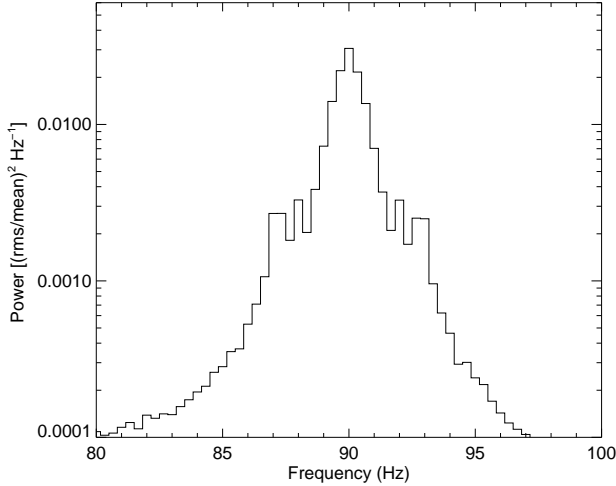


FIG. 3.— Feature produced by a sinusoidal oscillation with amplitude 0.1 and frequency 90 Hz added to the phase for the light curve profile of SGR 1806–20.

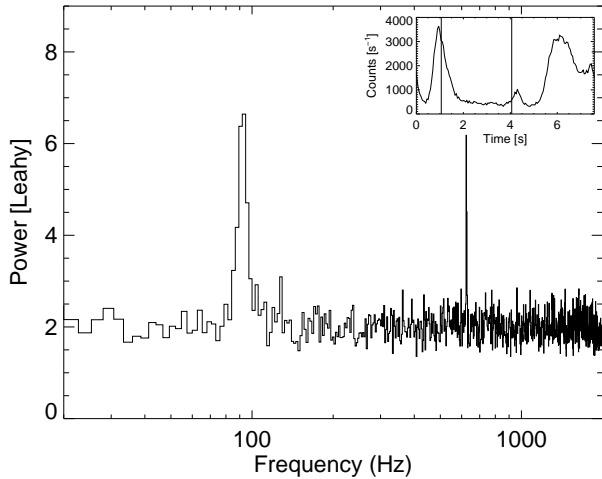


FIG. 4.— Main: power spectrum of a simulation using the SGR 1806-20 light curve (smoothed to a resolution of 0.1s). QPOs were inserted at 93 Hz and 626 Hz. Inset: the rotation-averaged pulse profile 195-260 s after the main flare. The section of the phase profile used in the power spectrum is marked by vertical lines.

with a width of 2 Hz. Both have an input amplitude of $|\Delta\Phi| = 0.1$. We use the same rotation phase as above, stack the power spectra from nine successive rotations and bin the data with a binsize of 2.66 Hz.

Figure 4 shows the power spectrum (in Leahy normalization) of one realization. The inset shows the averaged phase profile, with vertical lines denoting the phase segment used to make the power spectrum. This figure is comparable to Figure 2 of SW06. Both QPOs are visible by eye. In our spectrum the power above ~ 10 Hz has been removed from the smoothing applied to the light curve.

The QPO inserted at 93 Hz is detected with a mean width of 6.6 ± 1.5 Hz, rms amplitude of $21\% \pm 1.5\%$, and average central frequency of 91.7 ± 0.6 Hz. For the 626 Hz QPO, the mean width is 2.4 ± 1.4 Hz, with an rms amplitude of $15\% \pm 1.5\%$ and central frequency 624.9 ± 0.35 Hz.

The rms amplitude at 93 Hz is not significantly different from adding a sinusoid, but is measurably lower around

626 Hz. In both cases, however, the strength of the feature is significantly stronger than the underlying oscillation. The features show modest broadening with a large dispersion between different realizations. The systematic offset in the central frequency of the QPO appears because of the binsize. In simulations without photon noise, reducing the binsize shifts the central frequency of the QPO closer to the input one. Harmonics are not detected.

4. DISCUSSION

The steep pulse profile seen in the tail of giant magnetar flares substantially alters the observed properties of a starquake, changing both its observed amplitude and power distribution. While this effect is not large enough to transform a starquake with maximum amplitude $\Delta x/R_* \sim 0.001 - 0.01$ into a QPO with an rms amplitude of 20%, the boosting can still be considerable, especially if the emission comes from close to the rotation axis of the star, or if the steepest part of the beam gradient is misaligned with the viewing parallel (small α).

There are several uncertainties in our calculation that could boost the amplitude of a starquake further. The first of these is the unknown location of emission on the surface of the star. If the emission is close to the rotation axis, then a small physical motion produces a larger change in phase than at the equator. However, to produce a ten-fold increase requires an inclination angle of less than $\sim 6^\circ$, which is improbable given the strong observed pulsations.

The second way to boost the amplitude is for the beam to cross the observing parallel obliquely, as in Figure 1. Since in this case the actual beam edge is steeper than observed, the amplification is larger than expected from the observed beam shape. For the extreme case ($\alpha = 0$) the beam runs exactly parallel to the line of sight so that no pulse is seen but there is a strong QPO. This scenario is unlikely, both that α is so small and that the beam edge is so much sharper (by a factor $1/|\sin\alpha|$) than observed. As an example: to produce a feature with a rms amplitude of 20% requires a gradient $0.2 \sim dP/d\Phi \sim \langle P_0 \rangle A_0$ (cf. Equation (2)), which is $\sim 100\times$ steeper than the pulse profile in Figure 4.

The input amplitudes required to produce the strong QPOs of SGR 1806-20 are large enough to produce QPOs that are observable throughout the entire profile. Applying the model across the entire pulse profile (using 3s segments offset by $0.1P_*$ in phase), the oscillation has an output amplitude between 10% and 25%—strong enough to be detected throughout the rotation. If the emission model is correct, this requires that the starquake amplitude varies significantly across the surface of the crust and the correlation with the falling pulse edge is somewhat coincidental. This is expected generically in starquake models, however, and is seen directly in MHD simulations of coupled core-crust oscillations (Gabler et al. 2011) which show a strong phase dependence in the starquake amplitude.

The toy model suggests that the pulse profile can substantially influence the observed amplitude and other properties of a starquake. While we have used a simple model for the emission and starquake, this work can be easily generalized to use a physically-motivated model of the surface emission and starquake, in order to put constraints on the pattern of emission on the surface of the star during the quake.

We thank Phil Uttley, Yuri Levin and Daniela Huppenkothen for useful discussion and acknowledge support from an NWO Vidi Grant.

REFERENCES

- Duncan, R. C. 1998, *ApJ*, 498, L45
- Gabler, M., Cerdá Durán, P., Font, J. A., Müller, E., & Stergioulas, N. 2011, *MNRAS*, 410, L37
- Glampedakis, K., Samuelsson, L., & Andersson, N. 2006, *MNRAS*, 371, L74
- Israel, G. L., Belloni, T., Stella, L., et al. 2005, *ApJ*, 628, L53
- Levin, Y. 2006, *MNRAS*, 368, L35
- Levin, Y., & van Hoven, M. 2011, *MNRAS*, 418, 659
- Strohmayer, T. E., & Watts, A. L. 2005, *ApJ*, 632, L111
- . 2006, *ApJ*, 653, 593
- Thompson, C., & Duncan, R. C. 1995, *MNRAS*, 275, 255
- . 2001, *ApJ*, 561, 980
- Timmer, J., & Koenig, M. 1995, *A&A*, 300, 707
- Timokhin, A. N., Eichler, D., & Lyubarsky, Y. 2008, *ApJ*, 680, 1398
- van der Klis, M. 1989, in *Timing Neutron Stars*, ed. H. Ögelman & E. P. J. van den Heuvel, 27
- Watts, A. L. 2011, arXiv:1111.0514
- Watts, A. L., & Strohmayer, T. E. 2006, *ApJ*, 637, L117